Polysaccharide-water interactions: NMR and DVS data

Xavier Falourd, Corinne C. Rondeau-Mouro, Mireille Cambert, Marc Lahaye, Brigitte Chabbert, Véronique Aguié-Béghin

Data in Brief 53 (2024) 110106

Contents lists available at ScienceDirect

Data in Brief

journal homepage: www.elsevier.com/locate/dib

Data Article

Polysaccharide-water interactions: NMR and DVS data

X. Falourd [a,c,*], C. Rondeau-Mouro [b], M. Cambert [b], M. Lahaye [a], B. Chabbert [d], V. Aguié-Béghin [d]

[a] INRAE, UR1268 BIA, Nantes F-44316, France
[b] INRAE, UR1466 OPAALE, 17 Avenue de Cucillé, CS 64427, Rennes F-35044, France
[c] INRAE, BIBS Facility, PROBE Infrastructure, Nantes F-44316, France
[d] Université de Reims Champagne-Ardenne, INRAE, FARE, UMR A614, Reims, France

ARTICLE INFO

Article history:
Received 16 September 2023
Revised 9 January 2024
Accepted 22 January 2024
Available online 7 February 2024

Dataset link: Celluloses and konjac glucomannan assemblies TD-NMR, solid-state NMR and Dynamic Vapor Sorption datasets (Original data)

Keywords:
VCT-CPMAS
M_2
Park's model
Cellulose
Konjac glucomannan
Relaxation

ABSTRACT

The data provided here relate to the research paper "Assessing the complementarity of TD-NMR, solid-state NMR and Dynamic Vapor Sorption in the characterization of polysaccharide-water interactions". The original data from TD-NMR, ss-NMR and DVS is provided in .dps, topspin and .xls formats respectively, allowing other authors to repeat our processing protocols using different parameters. We also include results obtained by varying the signal treatments. The analysis of these multimodal data have highlighted a variation in polysaccharide-water interactions depending on the type of assembly. These datasets are very useful for discriminating between water bound to polysaccharides and water absorbed or adsorbed into polysaccharide network, a key element in understanding interactions in these assemblies and an essential approach for developing tailor-made polysaccharides-based products.

DOI of original article: 10.1016/j.carbpol.2023.121579
* Corresponding author at: INRAE, UR1268 BIA, Nantes F-44316, France.
E-mail address: xavier.falourd@inrae.fr (X. Falourd).

https://doi.org/10.1016/j.dib.2024.110106

Specifications Table

Subject	Materials Science - Biomaterials
Specific subject area	The role of water in the structuring and hygroscopic behaviour of cellulose based assemblies
Data format	Raw, Analyzed
Type of data	Table, Image, Chart, Graph, Figure
Data collection	Time Domain Nuclear Magnetic Resonance (TD-NMR) with minispec Bruker 20 MHz. Solid-state- NMR (ss-NMR) with 400 MHz Avance III. Dynamic Vapour Sorption (DVS) with SPSx-1μ, ProUmid.
Data source location	Institution: INRAE Town/City : TD-NMR (Rennes), ss-NMR (Nantes), DVS (Reims) Country : France
Data accessibility	Repository name: recherche.data.gouv Data identification number: 10.57745/4ZWXYH Direct URL to data: https://entrepot.recherche.data.gouv.fr/dataset.xhtml?persistentId=doi:10.57745/4ZWXYH
Related research article	Falourd, X., Rondeau-Mouro, C., Cambert, M., Lahaye, M., Chabbert, B. & Aguié-Béghin, V. Assessing the complementarity of TD-NMR, solid-state NMR and Dynamic Vapor Sorption in the characterization of polysaccharide-water interactions 10.1016/j.carbpol.2023.121579

1. Value of the Data

- TD-NMR, ss-NMR and DVS data provide a comprehensive picture of the dynamics and strength of water-polysaccharide interactions.
- The data could benefit research on bio-based materials.
- The data enable understanding of the hygroscopic behaviors of different polysaccharides assemblies.
- The data could be useful to develop new biodegradable bio-based food packaging.

2. Data Description

The present data have been acquired as part of a project aimed at gaining a better understanding of the role of water in the structuring and hygroscopic behavior of cellulose based assemblies. In this study, single and binary film formulations of cellulose and/or konjac glucomannan (KGM) were produced and conditioned (for NMR measurements) in atmospheres with different water activity (a_w) levels in order to obtain different water content values (see Table 1 column 1 and paragraph 2.1). These samples were analyzed by Dynamic Vapor Sorption (DVS), giving a sorption curve modelled according to Park's model (see Eq. (2)) with calculated deviation modulus E (see Eq. (3)), and a desorption curve that allowed the degree of hysteresis (dH, Eq. (1) in [1]) to be determined. All values obtained are reported in Table 2. The degree of hysteresis (dH) expresses the water retention of different films as a function of water content (see Fig. 1). To complement the classic T_2 relaxation times, TD-NMR was used to determine the second dipole moment M_2, which provides information on the strength and number of dipolar interactions between polysaccharide chains (see Fig. 2). Solid state NMR analysis provided ^{13}C spectra characteristic of the films' molecular structures (see Fig. 3). The degree of crystallinity of the polysaccharides was determined for each film (see Table 3). The ^{1}H->^{13}C polarization transfer kinetics for all signals are shown for films conditioned to $a_w = 0.59$ (see Fig. 4) and $a_w = 0.33$ (see Fig. 5). These kinetics were modelled so that the interactions and molecular organization could be characterized (see Table 4). A spectral deconvolution approach was used to depict and model the individual polarization transfer kinetics for cellulose and KGM (see Fig. 6 and Table 5).

Table 1
List of samples analyzed and names of corresponding datasets.

Sample identifier Polysaccharide(s) /w-w/ water activity	ss-NMR dataset	TD-NMR dataset	DVS dataset
CNF/0.33	CNF0_AW0.33.20220304	CNF-33	CNF film
CNF/0.59	CNF0_aw0.59.20220225	CNF07-59	
		CNF15-59	
		CNF17-59	
CNF/0.85	CNF0_AW0.86.20220311	CNF-85	
CNC/0.33	CNC0_AW0.33.20220307	CNC-33	CNC film
CNC/0.59	CNC_aw0.59.20220228	CNC-59	
CNC/0.85	CNC0_AW0.86.20220314	CNC-85	
KGM/0.33	GMK_02_AW0.33.20220525	GMK-33	KGM film
KGM/0.59	GMK_02_AW0.59.20220520	GMK59	
KGM/0.85	GMK_02_AW0.85.20220523	GMK85	
CNF KGM/2-1/0.33	CNF_GMK_2.1_AW0.33.20220316	CNFGMK-2-1-33	CNF-KGM/2-1
CNF KGM/2-1/0.59	CNF_GMK_2.1_AW0.59.20220318	CNFGMK-2-1-59	
CNF KGM/2-1/0.85	CNF_GMK_2.1_AW0.86.20220321	CNFGMK-2-1-85	
CNF KGM/1-2/0.33	CNF_GMK_02_AW0.33.20220502	CNFGMK-1-2-33	CNF-KGM/1-2
CNF KGM/1-2/0.59	CNF_GMK_02_AW0.59.20220427	CNFGMK-1-2-59	
CNF KGM/1-2/0.85	CNF_GMK_02_AW0.85.20220425	CNFGMK-1-2-85	
CNC KGM/2-1/0.33	CNC_GMK_2.1_AW0.33.20220323	x	CNC-KGM/2-1
CNC KGM/2-1/0.59	CNC_GMK_2.1_AW0.59.20220325	x	
CNC KGM/2-1/0.85	CNC_GMK_2.1_AW0.86.20220330	x	
CNC KGM/1-2/0.33	CNC_GMK_02_AW0.33.20220429	x	CNC-KGM/1-2
CNC KGM/1-2/0.59	CNC_GMK_02_AW0.59.20220420	x	
CNC KGM/1-2/0.85	CNC_GMK_02_AW0.85.20220422	x	

Table 2
Park's parameters calculated from Eq. (2). Mean relative percentage of deviation modulus E calculated from Eq. (3). (*) Data selected in Park's model for KGM and CNC-KGM (1-2). Corresponding fitting results are shown in parentheses.

Films	Park's parameters					
	AL	BL	KH	Ka	n	E
	(g/g)		(g/g)	(g/g)		(%)
CNC	0.017	15.9	0.082	0.162	5.3	1.54
CNF	0.027	22.1	0.102	0.154	5.6	0.93
KGM	0.024	25*	0.219	0.246	7.4	12.6*
		($1.1\ 10^{23}$)				1.01
CNC-KGM(2-1)	0.020	38.0	0.111	0.148	6.5	0.7
CNC-KGM(2-1)	0.018	80*	0.162	0.170	7.3	9.5
		($2.5\ 10^{35}$)				1.69
CNF-KGM(2-1)	0.025	36.1	0.129	0.164	6.2	2.08
CNF-KGM(1-2)	0.026	72.3	0.168	0.207	6.7	0.39

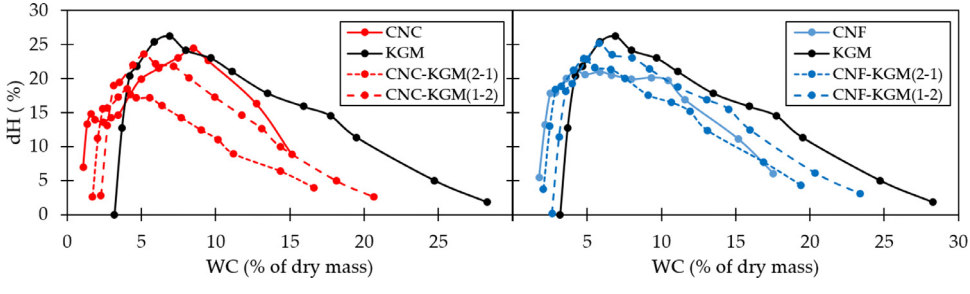

Fig. 1. Degree of hysteresis (dH) of pure (CNC, CNF, KGM) and binary (CNC-KGM and CNF-KGM) polysaccharidic films (binary weight ratios = (2-1) and (1-2) respectively), as a function of water content (WC (% of dry mass)).

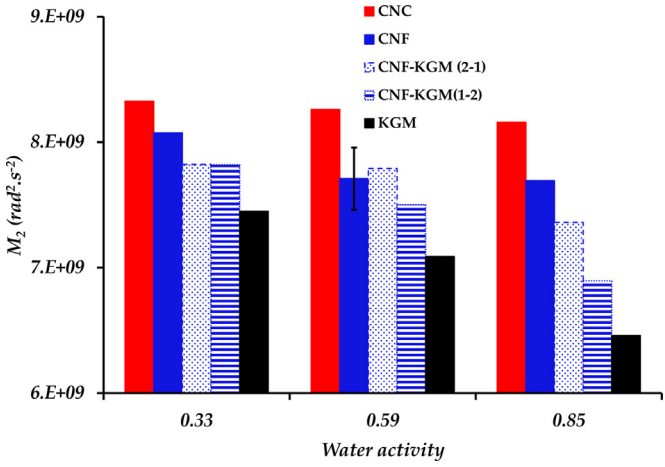

Fig. 2. TD-NMR evolution of the second dipole moment M_2 at 20°C for each film as a function of water activity. The standard deviation determined for CNF is shown.

Table 3
Crystallinity index of each films as a function of water activity.

aw	CNC	KGM	CNC-KGM (2-1)	CNC-KGM (1-2)	CNF	CNF-KGM (2-1)	CNF-KGM (1-2)
0.33	70%	0%	57%	37%	42%	35%	21%
0.59	71%	0%	59%	36%	43%	35%	21%
0.85	72%	0%	62%	37%	44%	38%	22%

Table 1 shows all sample experiments, which can be found in the database. The DVS dataset consists of DVS raw data files named by the film polysaccharide composition code and are grouped in a file named DVS dataset.tab. The TD-NMR dataset consists of NMR raw data files named by combining the film polysaccharide composition code with the relative humidity value used for conditioning prior to measurement by NMR. These raw files are in an archive named TD-NMR dataset.zip. The ss-NMR dataset consists of NMR raw data files named by the film composition code, the relative humidity used for conditioning prior to measurement by NMR and 8 digit format YYYYMMDD (Y=year, M= month, D=day). These raw files are in an archive named ss-NMR dataset.zip.

The entries in the first column describe the samples analyzed, comprising the polysaccharides that form the films (CNF = Cellulose NanoFibrils, CNC = Cellulose NanoCrystals and KGM = Konjac GlucoMannan), their relative proportions by mass in the case of binary films (2-1 or 1-2), and the water activity level of the conditioning atmosphere (0.33, 0.59 or 0.85). The second, third and fourth columns show the names of the associated ss-NMR, TD-NMR and DVS datasets respectively. TD-NMR data contain five files (_001 to _005) for each dataset, corresponding to the five temperatures studied as follows:

10°C	***_001***
20°C	***_002***
40°C	***_003***
60°C	***_004***
80°C	***_005***

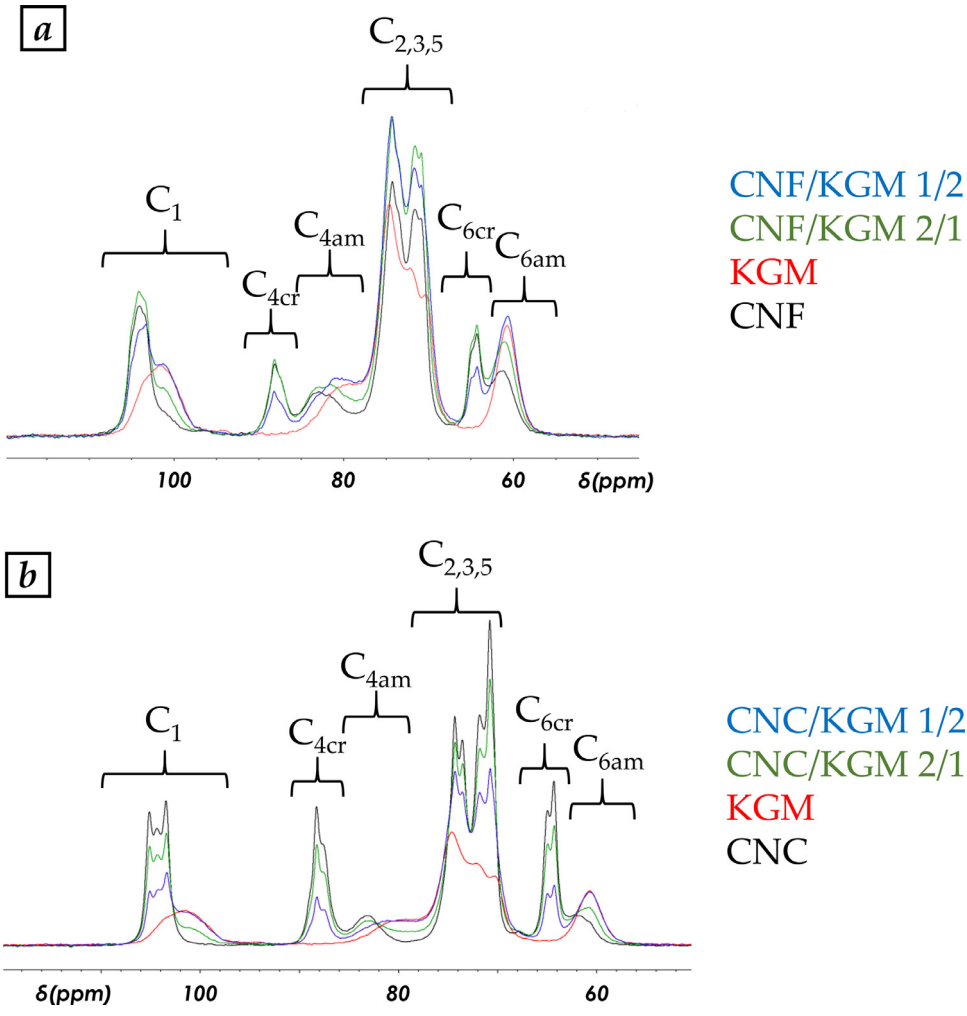

Fig. 3. ss-NMR: superimposition of ^{13}C CPMAS spectra obtained for (a) single and binary films based on CNF and (b) single and binary films based on CNC. All samples were prepared at $a_w = 0.85$.

3. Experimental Design, Materials and Methods

3.1. Sample Preparation for NMR Measurements

Single- and binary-polymer formulations were prepared from the respective cellulosic suspensions (CNC and CNF) and hemicellulosic solution (KGM) in different ratios, as described in [1]. Prior to measurement by NMR, the water content of all samples was adjusted using vapor phase isotopic equilibration with saturated salt solutions. These solutions produced relative partial water vapor pressures of 0.33, 0.59 and 0.85 using $MgCl_2$, NaBr and KCl, respectively at 20 +/- 0.1°C.

For TD-NMR, after 10 days, once thermodynamic equilibrium was obtained, respective relative partial pressure was considered to be equivalent to water activity (a_w) in both salt and polysaccharide phases. Between 200 and 300 mg of sample were used for TD-NMR analyses.

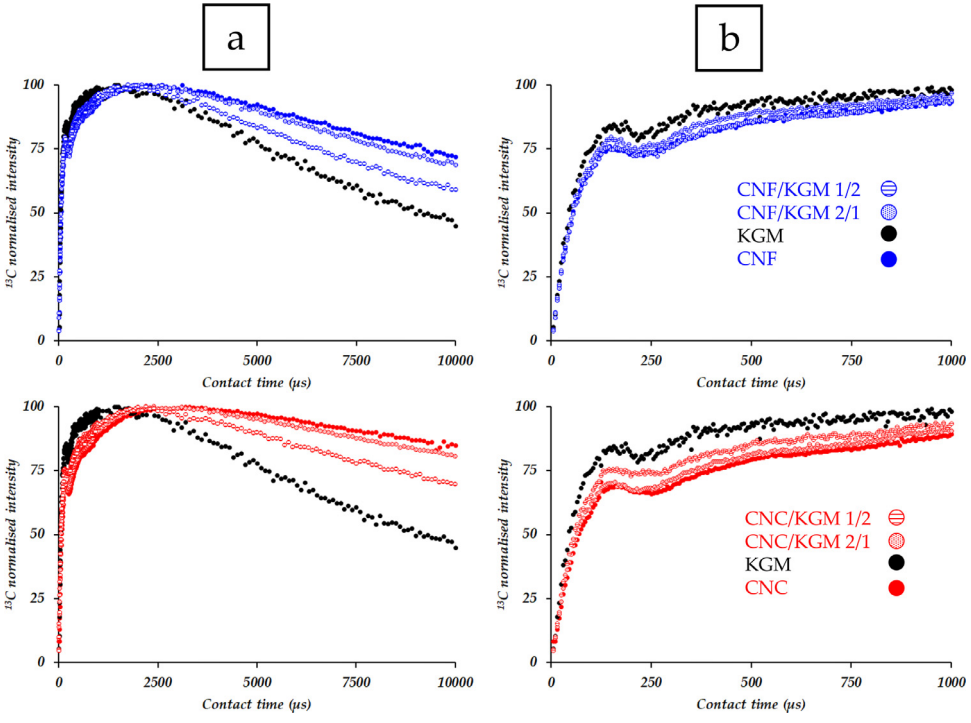

Fig. 4. VCT-CPMAS ^{13}C NMR kinetics for the sum of C1 to C5 signals for samples conditioned at aw = 0.59. The upper graphs show curves for single and binary films based on CNC and the lower graphs show curves for single and binary films based on CNF.

For ss-NMR, the water content of all samples was adjusted as described above for a minimum of 72 h. Equilibrium was achieved more quickly than for TD-NMR because of smaller sample sizes. Indeed, about 100 mg of each sample were packed in a 4 mm diameter rotor.

Due to the substantial amount of material required for these measurements, they could not be repeated during this project, except for CNF TD-NMR data.

3.2. DVS

A gravimetric sorption high speed analyzer (SPSx-1µ, ProUmid, Germany) was used to identify the water sorption-desorption isotherms in each film (~100 mg). This DVS equipment can continuously analyze eleven samples at once. The latter were kept at a controlled temperature (20°C) in a chamber with an air flow of 5 $L.min^{-1}$ with a controlled moisture content ranging from 2 to 90% relative humidity (RH) corresponding to water activity levels of 0.02–0.9. The sample holder and counterweight were connected to an ultra-sensitive microbalance (± 1 µg precision). Sample mass was recorded every 10 min. throughout the process (sorption and desorption cycle) until equilibrium was reached at each RH. At this stage, sample mass was equal to at least 99% of the value of the asymptote of the mass vs time curve.

Water content (WC, %) was calculated according to the following Eq. (1):

$$WC\ (\%) = 100\ x\ -m_d/m_d \quad (1)$$

where m_{eq} is the mass of the sample at the equilibrium state, and m_d is the mass of the dry sample measured following a drying sequence. The drying sequence consisted of a heating step at 40°C under a dry flow of air for 24 h followed by a cooling step at 20°C.

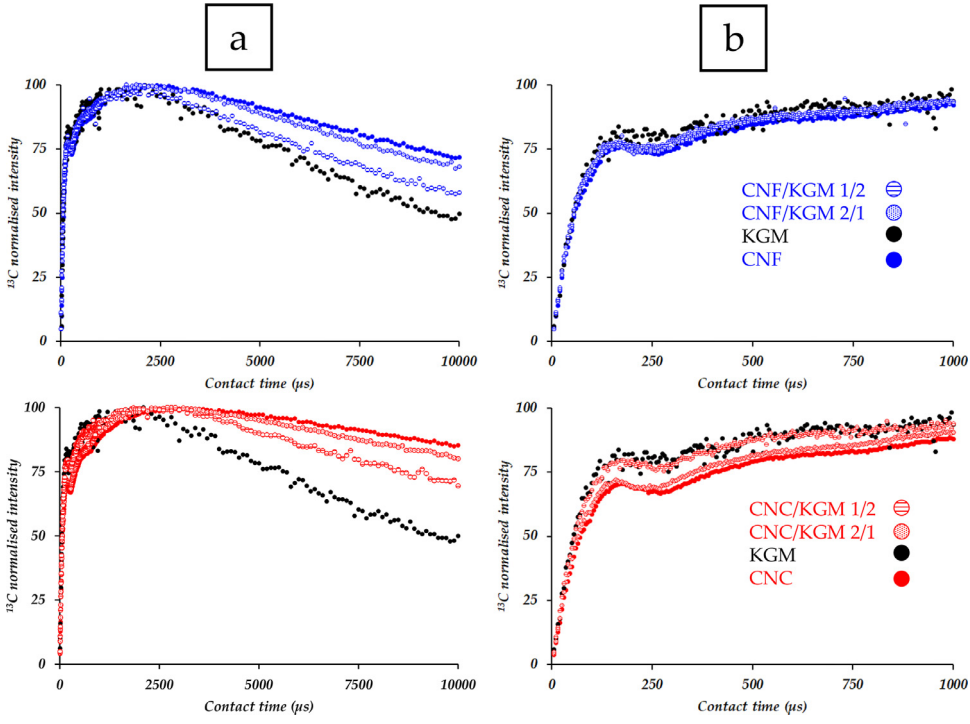

Fig. 5. VCT-CPMAS ^{13}C NMR kinetics for the sum of C1 to C5 signals for samples conditioned at a_w = 0.33. The upper graphs show curves for single and binary films based on CNC and the lower graphs show curves for single and binary films based on CNF.

The water sorption curves were converted as a function of water activity levels (a_w) and fitted using the model proposed by Park [2] according to Eq. (2):

$$Cwp_s = \frac{A_L \times B_L \times a_w}{1 + B_L \times a_w} + K_H \times a_w + K_a \times a_w^n \quad (2)$$

where Cwp_s is the calculated water content during the sorption step, expressed in g of water per g of dry sample; A_L is the concentration of water-specific sorption sites within a single layer; and B_L, is the water affinity concentration for these sites at low water activity, i.e. $a_w < 0.1$. K_H, the Henry's Law constant, expresses the affinity of water molecules in specific water sites and the random adsorption of water in multilayers in a 0.1-0.7 a_w range within the amorphous phase of the film material. K_a, the aggregation equilibrium constant, and n the number of water molecules in aggregates for $a_w < 0.7$, express the aggregation of condensed water in microcapillary cavities. According to Park's model, which is used to fit the sorption curves, five parameters can be employed to assess water behavior during sorption: A_L, B_L, K_H and K_a and n.

Isotherm fitting was evaluated in terms of the mean relative percentage deviation modulus E, which was calculated according to the following Eq. (3):

$$E = \frac{100}{N} \sum \frac{C_{wi} - C_{wpi}}{C_{wi}} \quad (3)$$

where *Cwi* is the experimental water content value, *Cwpi* is the calculated water content using the Park model, and N is the number of experimental data points. E values lower than 2 indicate a better fit.

Table 4
Proton diffusion and relaxation values obtained by modelling the proton transfer kinetics of the different films with different water contents.

			Equation 6			Equation 7		
		WC (%)	T_{HHa1} (μs)	T_{HHb} (μs)	∇	T_{HHa2} (μs)	T_{HHc} (μs)	T_{CH} (μs)
aw=0.85	CNC	15.1	57	366	0.49	64	768	43
	KGM	28.3	68	238	0.58	71	1279	59
	CNC/KGM 2/1	16.6	60	349	0.52	68	790	46
	CNC/KGM 1/2	20.7	61	326	0.55	67	840	52
	CNF	17.5	65	364	0.55	70	937	54
	KGM	28.3	68	238	0.58	71	1279	59
	CNF/KGM 2/1	19.4	62	345	0.56	66	920	54
	CNF/KGM 1/2	23.4	58	277	0.56	62	847	51
aw=0.59	CNC	7.4	73	449	0.53	76	1042	58
	KGM	15.9	59	263	0.62	65	1004	58
	CNC/KGM 2/1	9.0	65	458	0.54	71	945	54
	CNC/KGM 1/2	11.7	64	394	0.60	70	979	59
	CNF	9.5	61	397	0.58	65	967	56
	KGM	15.9	59	263	0.62	65	1004	58
	CNF/KGM 2/1	10.7	65	391	0.58	70	981	57
	CNF/KGM 1/2	13.1	64	324	0.58	68	886	55
aw=0.33	CNC	4.2	71	500	0.57	81	1116	61
	KGM	9.7	80	281	0.59	78	1228	59
	CNC/KGM 2/1	5.6	64	484	0.54	76	1008	56
	CNC/KGM 1/2	7.2	73	330	0.60	71	1077	67
	CNF	5.8	70	405	0.60	73	1110	61
	KGM	9.7	80	281	0.59	78	1228	59
	CNF/KGM 2/1	6.6	74	349	0.56	74	968	55
	CNF/KGM 1/2	8.0	67	331	0.61	65	1023	62

3.3. TD-NMR

M_2 measurements of films were performed using a minispec 20-MHz Bruker spectrometer (Wissembourg, France). The conditions and sequence used for measurements are described in [1]. The fitting of the FID-CPMG signals required the combination of exponential, Gaussian and SinC functions and was performed using both discrete and continuous methods (TableCurve software and Emilio-FID software©) as described in Ying et al. [3].

Second moment M_2 values were calculated from the wide part of the FID curve produced by protons in the solid fraction using Eq. (4) [4]:

$$I_{(t)} = Ae^{\left(-\frac{a^2 \times t^2}{2}\right)} \times \frac{\sin bt}{bt} \quad (4)$$

In this equation, I(t) is the evolution of the signal intensity in function of time, parameter A represents the proton fraction (normalized to 100% for the whole signal) associated with the shortest T_2 relaxation time. The NMR spectrum of the immobile proton fraction is assumed to have a rectangular line shape with a total width of 2b, which is convoluted with a gaussian

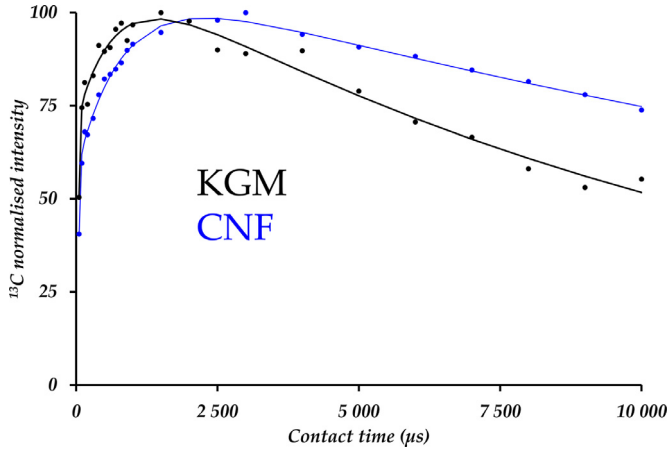

Fig. 6. ss-NMR VCT experimental and modelled data following deconvolution of CNF-KGM film conditioned at $a_w = 0.85$.

Table 5
Proton diffusion and relaxation values obtained by modelling the kinetics from the deconvoluted spectra.

			Cellulose Equation 8				GMK Equatio		
		WC (%)	T_{HH} (µs)	T_{CH} (µs)	$T_{1\rho}{}^{H}$ (ms)	lambda	T_{HH} (µs)	T_{CH} (µs)	T_1
aw=0.85	CNC	15.1	794	32	43.7	0.50			
	KGM	28.3					1168	37	
	CNC/KGM 2/1	16.6	813	34	41.7	0.49	376	37	
	CNC/KGM 1/2	20.7	811	34	33.8	0.50	1204	35	
	CNF	17.5	1106	40	27.6	0.45			
	KGM	28.3					1168	37	
	CNF/KGM 2/1	19.4	844	36	24.9	0.49	710	35	
	CNF/KGM 1/2	23.4	961	33	17.4	0.49	1024	33	
aw=0.59	CNC	7.4	965	39	34.5	0.49			
	KGM	15.9					802	37	
	CNC/KGM 2/1	9.0	964	36	39.7	0.47	714	35	
	CNC/KGM 1/2	11.7	1169	36	26.8	0.52	602	36	
	CNF	9.5	948	35	23.4	0.47			
	KGM	15.9					802	37	
	CNF/KGM 2/1	10.7	855	36	25.8	0.49	1100	38	
	CNF/KGM 1/2	13.1	768	40	22.1	0.48	780	34	
aw=0.33	CNC	4.2	998	37	39.3	0.48			
	KGM	9.7					1418	37	
	CNC/KGM 2/1	5.6	1071	37	31.1	0.50	946	40	
	CNC/KGM 1/2	7.2	945	40	31.2	0.49	1115	37	
	CNF	5.8	1043	44	24.0	0.49			
	KGM	9.7					1418	37	
	CNF/KGM 2/1	6.6	815	37	25.7	0.50	951	34	
	CNF/KGM 1/2	8.0	795	37	22.0	0.49	798	32	

function using a standard deviation given by parameter a. Triplicates could be studied only for CNF conditioned at a water activity level of 0.59 (the only sample of which there was sufficient quantity with the same water content). These correspond to the three datasets CNF07, CNF15 and CNF17.

The second dipole moment, which is a measure of the number and/or strength of the dipolar interactions in hydrogen, is calculated from fitting parameters a and b using the following Eq. (5):

$$M_2 = a^2 + \frac{1}{3}b^2 \tag{5}$$

As Fig. 2 shows, M_2 was proportional to the content of each component in the case of binary assemblies. The higher the level of KGM in the binary assemblies, the lower the M_2 was observed to be. Moreover, M_2 tended to decrease with increasing water content. This decrease of M_2 with an increase in water content indicated lower proton dipolar strength or lower proton density due to an increase in the average distances between the polysaccharide protons and/or in their mobility [5]. This phenomenon was heightened in KGM and the binary assemblies while the CNC and CNF films were less sensitive to changes in hydration.

3.4. ss-NMR

ss-NMR spectra were acquired on a Bruker Advance III 400 spectrometer as described in [1]. ^{13}C-CPMAS spectra were acquired to characterize polysaccharide structures.

The crystallinity index for films was determined according to the method proposed by Larsson et al. [6]. For binary films, C4 associated with KGM were included in the amorphous fraction.

Based on our previous work, the kinetics of 300 points were obtained using 128 accumulations and a recovery time of 3 s (Falourd et al., 2022b).

Modelling of the total kinetics was performed using the two Eqs. (6) and (7) previously proposed [7]:

$$I(\tau) = I_0\left(1 - \nabla\, e^{-\tau/T_{HHa1}} - (1-\lambda)e^{-\tau/T_{HHb}} \times cos\left(\frac{\pi}{2}b\tau\right)\right) \tag{6}$$

$$I(\tau) = I_0 e^{-\tau/T_{1\rho}^{H}}\left(1 - \lambda\, e^{-\tau/T_{HHa2}} - (1-\lambda)e^{-\tau/T_{HHc}} \times e^{-\tau^2/2T_{CH}^2}\right) \tag{7}$$

where, $I(\tau)$ is the intensity of the carbon peaks as a function of contact time τ and I_0 is the maximum intensity of the same carbons (associated with optimal contact time). T_{HHa1} and T_{HHb} are the two components of the spin diffusion process, ∇ defines the proportion of these two T_{HH} and b is the dipole coupling that depends on the angle between the static magnetic field and the vector between the ^{13}C and ^{1}H nuclei in Eq. (6). T_{HHa1}, T_{HHb} and ∇ are replaced by T_{HHa2}, T_{HHc} and λ in Eq. (7). $T_{1\rho}{}^{H}$ (spin lattice relaxation time in rotating frame) provides information on the molecular order within a sphere of a few tens of nanometers in diameter surrounding the carbons studied [8].

To model individual kinetics following deconvolution, a simpler equation with only one spin diffusion time was used:

$$I(\tau) = I_0 e^{-\tau/T_{1\rho}^{H}}\left(1 - \lambda\, e^{-\tau/T_{HH}} - (1-\lambda)e^{-3\tau/2T_{HH}} \times e^{-\tau^2/2T_{CH}^2}\right) \tag{8}$$

4. Conclusion

The data obtained from the three analytical methods used in this work have been shown to be highly sensitive to the polysaccharide composition and water contents of the studied assemblies. These data are well-suited for assessing polysaccharide-water interactions in bio-sourced

materials and should give new insights into the organization of water molecules in cellulose based assemblies in different humidity conditions.

Limitations

Due to the scarcity of samples, the primary limitation of this study is the absence of measurement repetitions. However, given the acknowledged robustness, it is common to proceed in such a manner, considering the substantial signal acquisition times and the equally significant quantity of required samples.

Ethics Statement

This research does not involve animal or human samples and therefore requires no ethical approval.

Data Availability

Celluloses and konjac glucomannan assemblies TD-NMR, solid-state NMR and Dynamic Vapor Sorption datasets (Original data) (recherche.data.gouv).

CRediT Author Statement

X. Falourd: Conceptualization, Methodology, Formal analysis, Investigation, Data curation, Writing – original draft; **C. Rondeau-Mouro:** Conceptualization, Methodology, Investigation, Data curation, Writing – review & editing; **M. Cambert:** Formal analysis; **M. Lahaye:** Conceptualization, Methodology, Writing – review & editing; **B. Chabbert:** Conceptualization, Methodology, Writing – review & editing; **V. Aguié-Béghin:** Conceptualization, Methodology, Formal analysis, Investigation, Data curation, Writing – review & editing.

Declaration of Competing Interest

The authors declare that they have no known competing financial interests or personal relationships that could have appeared to influence the work reported in this paper.

References

[1] X. Falourd, C. Rondeau-Mouro, M. Cambert, M. Lahaye, B. Chabbert, V. Aguié-Béghin, Assessing the complementarity of time domain NMR, solid-state NMR and dynamic vapor sorption in the characterization of polysaccharide-water interactions, Carbohydr. Polym. 326 (2024) 121579, doi:10.1016/j.carbpol.2023.121579.
[2] F. Gouanvé, S. Marais, A. Bessadok, D. Langevin, C. Morvan, M. Métayer, Study of water sorption in modified flax fibers, J. Appl. Polym. Sci. 101 (2006) 4281–4289, doi:10.1002/app.23661.
[3] R. Ying, L. Saulnier, C. Rondeau-Mouro, Films of arabinoxylans and β-glucans extracted from cereal grains: molecular motions by TD-NMR, Carbohydr. Polym. 86 (2011) 812–822, doi:10.1016/j.carbpol.2011.05.033.
[4] A. Abragam, The Principles of Nuclear Magnetism, Oxford University Press, Oxford, 1961 Repr.
[5] I.J. Van Den Dries, D. Van Dusschoten, M.A. Hemminga, E. Van Der Linden, Effects of water content and molecular weight on spin probe and water mobility in malto-oligomer glasses, J. Phys. Chem. B 104 (2000) 10126–10132, doi:10.1021/jp0001541.
[6] P.T. Larsson, K. Wickholm, T. Iversen, A CP/MAS 13C NMR investigation of molecular ordering in celluloses, Carbohydr. Res. 302 (1997) 19–25, doi:10.1016/S0008-6215(97)00130-4.
[7] X. Falourd, M. Lahaye, C. Rondeau-Mouro, Assessment of cellulose interactions with water by ssNMR: 1H->13C transfer kinetics revisited, Carbohydr. Polym. 298 (2022) 120104, doi:10.1016/j.carbpol.2022.120104.
[8] A. Yuris, J. Hindmarsh, A.K. Hardacre, K.K.T. Goh, L. Matia-Merino, The interactions between wheat starch and Mesona chinensis polysaccharide: a study using solid-state NMR, Food Chem. 284 (2019) 67–72, doi:10.1016/j.foodchem.2019.01.098.